PAPR Reduction in OTFS by modified Similar Raised Cosine mSRC Pulse Shaping

Benadjina Nassim
Dept. of electrical engineering
Larbi Ben M'Hidi University
Oum El Bouaghi, Algeria.
nnassimm1983@yahoo.fr

Lashab Mohamed
Dept. of electrical engineering
Larbi Ben M'Hidi University
Oum El Bouaghi, Algeria.
lashabmoh@yahoo.fr

Slimani Djamel
Dept. of electronic
University of Setif 1
Setif, Algeria.
slimani.djamel@ymail.com

***Abstract*— In this letter, we analyze Peak-to-Average Power Ratio (PAPR) of orthogonal time-frequency space (OTFS) modulation with pulse shaping. We implemented modified similar raised cosine (mSRC) pulse shaping in the OTFS based System and compare it with rectangular and raised cosine (RC) pulse shaping. Simulations results show that the use of mSRC pulse shaping in OTFS based system reduces the PAPR significantly and achieves better performances maintaining BER performance compared to other pulses shaping.**

Keywords— OTFS, Peak-to-average power ratio (PAPR), Pulse Shaping PS, mSRC, delay-Doppler domain.

I. INTRODUCTION

Mobile communication systems are evolving from single carrier to orthogonal time frequency and space (OTFS) modulation [1].

Orthogonal time frequency and space (OTFS) modulation is a new type of modulation technique that can be used for low-latency wireless communication and high-quality data transmission [2, 3], it is a 2-dimensional modulation technique designed in delay-Doppler domain to efficiently handle the high Doppler sensitivity problem occurring in OFDM modulation and to achieve efficient data transfer in high-speed vehicular scenario. The main advantage of OTFS modulation is the use of orthogonal subcarriers. These are carriers at different frequencies which make it possible to send multiple streams of data simultaneously over the same signal bandwidth. Since OTFS modulation claims excellent performance and offers several advantages in doubly selective wireless channels, it seems to be one of those technologies that could change everything for next-generation communication systems.

However, OTFS is suffering from high PAPR problem for increasing number of symbols [4,6], it has been attracting considerable interest to study their PAPR characteristics for higher values of number of Doppler bins N. Several studies on PAPR of OTFS have been made in the literature [4-11].

Mathematical performance analysis of PAPR of OTFS has been presented in [4], where the authors derive an analytical upper bound on the PAPR, they demonstrated that this bound increases linearly with N and not with the number of delay bins M. Then, the effect of pulse shaping on the PAPR performance of OTFS system has been analyzed, they showed that Gaussian and raised cosine pulse shaping increases the PAPR of OTFS and OTFS can have better PAPR comparing to those of OFDM and GFDM. Authors in [5] proposed a novel interleaved time-frequency multiple access (ITFMA) scheme using OTFS on the uplink, this scheme was found to achieve good PAPR performance. In [11], the authors proposed a companding technique to reduce the PAPR of OTFS, but with slight degradation in BER performance. PAPR reduction method based on iterative clipping and filtering (ICF) was investigated in [12], this method found to reduce the PAPR with mild BER performance loss.

Reference [8] presents the first attempt to include pulse shaping in OTFS, the rectangular and prolate spheroidal pulse shaping were applied. The most first systems of OTFS have used a rectangular pulse shape [2,9-10]. Circular Dirichlet pulse shaped (CPS) is applied to reduce the out-of-band OOB power radiation in [11], the authors identified that this pulse shaped has a lower PAPR than conventional OTFS system.

To reduce high PAPR of OTFS signal in this paper, we use modified similar raised cosine (mSRC) pulse shaping which will reduce the PAPR of OTFS regarded to other existing pulses.

The similar raised-cosine (SRC) pulse was initially proposed in [12] and modified in [13] by adding a second design parameter β that provides an additional degree of freedom for a certain roll-off factor α, the mSRC corresponding time function is given by

$$p_{mSRC}(t) = \operatorname{sinc}\left(\frac{\beta t}{T_0}\right)\frac{1-2\cos\left(\pi\alpha\frac{t}{T_0}\right)}{(3\alpha t/T_0)^2-1} \qquad (1)$$

where, the parameter β is defined for all real numbers, α is the roll-off factor, T_0 is the symbol period. $t = nT_s$, where, n is the number of samples and T_s is the sampling frequency.

Fig. 1 represent the time domain function for modified similar raised cosine pulse shaping with α = 0.22 and different values of β.

II. UPLINK OTFS SYSTEMP

A. System Model

Each information symbols at the OTFS uplink transmitter are considered as points in two-dimensional delay-Doppler grid and are mapped to the time-frequency (TF) plane through the 2D inverse symplectic finite Fourier transform (ISFFT). The signal data obtained is then passed through a multicarrier modulation system. Then this signal is transformed to a time-domain signal and transmitted using Heisenberg transform. The output data of the Heisenberg transform are transmitted over the linear time-variant channel [4].

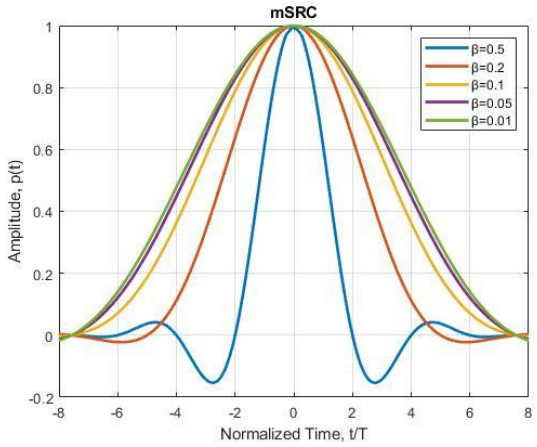

Fig. 1. Time function of mSRC pulse for α = 0.22 with β varies.

We consider $N \times T$ the total time duration of transmitted OTFS signal and $BW = M/T = M \times \Delta f$ the bandwidth occupied by the transmitted signal. The information symbols in delay-Doppler domain are represented using the notation $x[k,l], k = 0,1,\ldots,N-1, l = 0,1,\ldots,M-1$ and $x[k,l] \in A$, where A represents modulation data of one of various modulation schemes. Those modulation alphabet points are distributed to points in 2D delay-Doppler grid. These symbols are mapped to symbols in time-frequency plane by using a 2D transformation called inverse symplectic finite Fourier transform (ISFFT), that is given by

$$X_u[n,m] = \sum_{k=0}^{N-1}\sum_{l=0}^{M-1} x_u[k,l] e^{j2\pi\left(\frac{nk}{N}-\frac{ml}{M}\right)} \tag{2}$$

Then after passing the obtained TF signal via a multicarrier modulation system and a Heisenberg transformation, the time domain signal will get back from the time-frequency, which given by

$$s(t) = \sum_{n=0}^{N-1}\sum_{m=0}^{M-1} X[n,m] g_{tx}(t-nT) e^{j2\pi m\Delta f(t-nT)} \tag{3}$$

where $g_{tx}(t)$ represents the periodic prototype transmit pulse shape with total duration of $N \times T$. The discrete-time representation of (3) is obtained by applying sampling with $Fs = 1/Ts = BW$ sampling rate, that is given by

$$s(uT_s) = \sum_{n=0}^{N-1}\sum_{m=0}^{M-1} X[n,m] g_{tx}(uT_s-nT) e^{j2\pi m\Delta f(uT_s-nT)} \tag{4}$$

where $u = 0,1,\ldots,MN-1$. The Nyquist sampling with oversampling ratio = 1 for this description is considered. To represent the samples as $s(u), u = 0,1,\ldots,MN-1$ as an $N \times M$ matrix, assume $s(q,r)$ such that $u = r + qM$, where $r = 0,1,\ldots,M-1$ and $q = 0,1,\ldots,N-1$. Then by putting (2) in (4) with $u = r + qM$, the resulting equation is

$$(r+qM) = \sum_{n=0}^{N-1}\sum_{m=0}^{M-1}\sum_{k=0}^{N-1}\sum_{l=0}^{M-1} x[k,l] e^{-j2\pi\left(\frac{ml}{M}-\frac{nk}{N}\right)} g_{tx}([r + qM - nM]_{MN}) e^{j\frac{2\pi}{M}m(r+qM)} \tag{5}$$

In this, the mod-MN operation has represented by $[.]_{MN}$ confines the total duration of one frame transmission with in $N \times T$. The above equation can be further simplified as

$$s(r+qM) = \sum_{n=0}^{N-1}\sum_{m=0}^{M-1} x[k,l] \sum_{k=0}^{N-1} e^{\frac{j2\pi m}{M}(-l+r)} \sum_{l=0}^{M-1} g_{tx}([r + qM - nM]_{MN}) e^{j\frac{2\pi nk}{N}} \tag{6}$$

Now, defining $\mathcal{F} \triangleq \sum_{m=0}^{M-1} e^{\frac{j2\pi m}{M}(-l+r)}$, we note that

$$\mathcal{F} = \begin{cases} 0 & if\ r \neq l \\ M & if\ r = l \end{cases} \tag{7}$$

Substituting (7) in (6), we get

$$s(r+qM) = M \sum_{n=0}^{N-1}\sum_{k=0}^{N-1} x[k,r] e^{j\frac{2\pi nk}{N}} g_{tx}([r + qM - nM]_{MN}) \tag{8}$$

Observe that $\sum_{n=0}^{N-1} x[k,r] e^{j\frac{2\pi nk}{N}}$ is the n th ($n = 0,1,\ldots,N-1$) N-point IDFT of $x[k,r], k = 0,1,\ldots,N-1$, for a given r.

Denoting $\tilde{x}_r(n) = \sum_{n=0}^{N-1} x[k,r] e^{j\frac{2\pi nk}{N}}$, (8) can be written as

$$s(r+qM) = M \sum_{n=0}^{N-1} \tilde{x}_r(n) g_{tx}([r + qM - nM]_{MN}). \tag{9}$$

B. Maximum Bound on OTFS PAPR

Let's consider the samples of transmitted OTFS signal in equation (8). The Peak to Average Power Ratio of discrete OTFS time samples of transmit signal is defined as

$$PAPR = \frac{\max_{r,q}\{|s(r+qM)|^2\}}{P_{avg}} \tag{10}$$

where

$$P_{avg} = \frac{1}{MN}\sum_{r=0}^{M-1}\sum_{q=0}^{N-1} E\{|s(r+qM)|^2\} \tag{11}$$

The max bound of PAPR for the pulse shaped OTFS signal can be obtained as [4]

$$PAPR \leq \frac{M^2N^2 \max_{k,l}|x[k,l]|^2 B_1}{M^2N\sigma_a^2 B_2} \tag{12}$$

$$PAPR_{max} = \frac{N \max_{k,l}|x[k,l]|^2 B_1}{\sigma_a^2 B_2} \tag{13}$$

With $\sigma_a^2 = E\{|x[k,l]|^2\}$,

$$B_1 \triangleq \max_{r,q} \sum_{n=0}^{N-1} |g_{tx}([r + qM - nM]_{MN})|^2$$

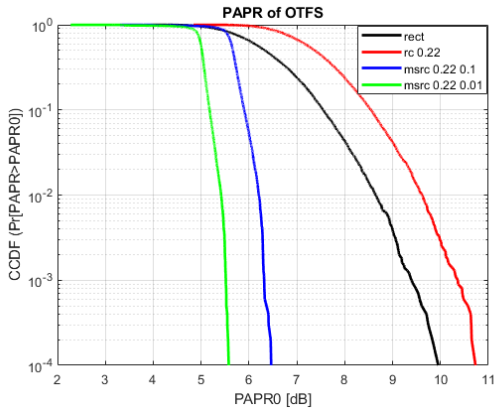

Fig. 2. CCDF of PAPR for pulse shaping OTFS with rectangular, RC, mSRC pulses and N=8, M=8, α = 0.22, and β = 0.1, 0.01.

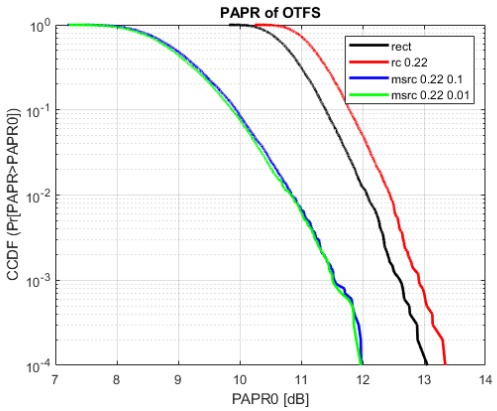

Fig. 3. CCDF of PAPR for pulse shaping OTFS with rectangular, RC, mSRC pulses and N=128, M=1024, α = 0.22, and β = 0.1, 0.01.

and,

$$B_2 \triangleq \frac{1}{MN}\sum_{n=0}^{N-1}\sum_{r=0}^{M-1}\sum_{q=0}^{N-1}|g_{tx}([r+qM-nM]_{MN})|^2$$

For rectangular pulse shape $\frac{B1}{B2}=1$, therefore the maximum PAPR will be delimited as,

$$PAPR \le \frac{M^2N^2 \max_{k,l}|x[k,l]|^2}{M^2N\sigma_a^2} \quad (14)$$

$$PAPR_{max} = \frac{N \max_{k,l}|x[k,l]|^2}{\sigma_a^2} \quad (15)$$

C. *CCDF (Complementary Cumulative Distribution Function) of OTFS PAPR*

The CCDF of PAPR of OTFS is given by [4]

$$P(PAPR \le \lambda_0) \approx 1-\left(1-e^{\lambda_0}\right)^{MN} \quad (16)$$

where λ_0 is the threshold value when the probability that PAPR of OTFS transmitted signal per one frame not exceed.

III. RESULTS AND DISCUSSIONS

Figure 2 shows the comparison of simulated CCDF of PAPR of OTFS system with mSRC, RC and rectangular pulses using 16-QAM for M=8 and N=8, α=0.22, β=0.1,0.01, and the pulses are four times oversampled with a length of 8T. We observed that the use of mSRC pulse shaping reduces the PAPR of OTFS compared to rectangular and RC pulses. For example, the PAPR of OTFS with mSRC pulse shaped is 4 dB lower than that with rectangular pulse shaped for β=0.01 at a probability of 10^{-3} and 3 dB lower for β=0.1. We found that using β with small values improves the performance of PAPR of OTFS with mSRC pulse shaping.

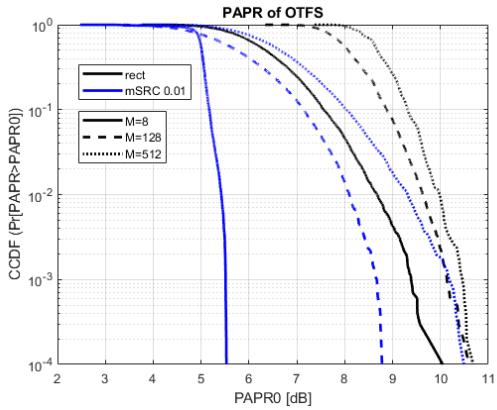

Fig. 4. CCDF of PAPR for pulse shaping OTFS with rectangular and mSRC pulses for N=8, α = 0.22, and β = 0.1, 0.01 when M varies.

Figure 3 shows the comparison of simulated CCDF of PAPR of OTFS system with mSRC, RC and rectangular pulses using 16-QAM for M=1024 and N=128, α=0.22, β=0.1,0.01 and the pulses are four times oversampled with a length of 8T. We observed that mSRC pulse shaping still reduces the PAPR of OTFS compared to rectangular and RC. But unlike for smaller value off N and M, the PAPR is 1dB lower with mSRC compared to rectangular pulse and the curve of PAPR with mSRC for β=0.01 is closer to that for β=0.1 (for N=8 and M=8, PAPR with mSRC for β=0.01 is almost 1dB lower at probability of 10^{-3} regarded to PAPR for β=0.1).

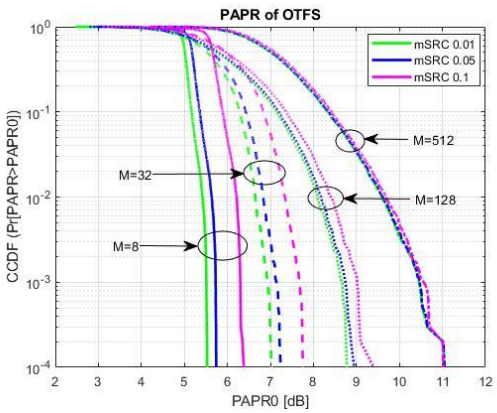

Fig. 5. CCDF of PAPR for pulse shaping OTFS with mSRC for N=8, α = 0.22 when M and β vary.

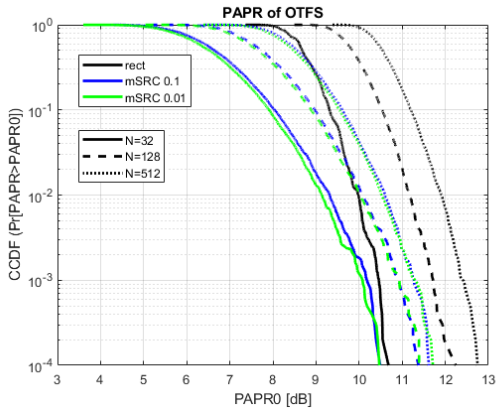

Fig. 6. CCDF of PAPR for pulse shaping OTFS with rectangular and mSRC pulses for M=512, α = 0.22 and β = 0.1, 0.01 when N varies.

Figure 4 shows the effect of mSRC pulses when M varies on the simulated CCDF of PAPR of pulse shaped OTFS system regarding rectangular pulse using 16-QAM for N=8 and α=0.22. For small values of M, there is a large distance between PAPR curves of mSRC and rectangular. When the values of M increase, this distance decreases.

Figure 5 shows the effect of β when M varies on the simulated CCDF of PAPR of pulse shaped OTFS system with mSRC using 16-QAM for N=8 and α=0.22. For small values of M, there is a large distance between PAPR curves for different values of β. When the values of M increase, this distance decreases until it vanishes so that changing the values of B does not affect the shape of PAPR.

Figure 6 shows the effect of β when N varies on the simulated CCDF of PAPR of pulse shaped OTFS system with mSRC and rectangular pulses using 16-QAM for M=512 and α=0.22. We note that when the values of N change, the variation of β does not affect the PAPR curves of mSRC, the curves are close to each other, but when N increases the distance of PAPR curves between the mSRC and rectangular pulses increases.

Figure 7 shows the comparison of simulated BER of pulse shaped OTFS system with mSRC pulse shaping and rectangular pulse for 16-QAM, M=32 and N=8, α=0.22, β=0.1,0.01. We observed that the BER curves of simulated pulse shaping is closer to the curve of original of OTFS.

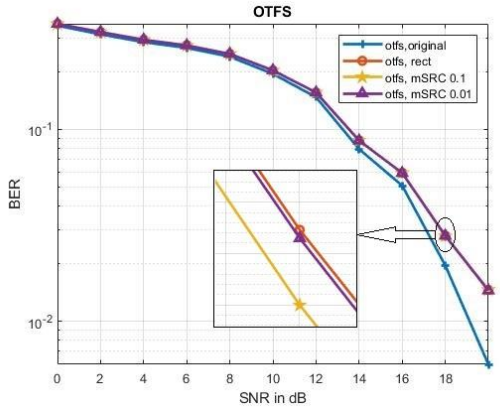

Fig. 7. BER performance of rectangular, mSRC pulse shaping OTFS based system with M = 32, N = 8, α = 0.22, and B= 0.1, 0.01.

IV. CONCLUSIONS

We proposed the use of modified similar raised cosine (mSRC) pulse shaping in OTFS based systems. This pulse shaping scheme was found to achieve better PAPR performance compared to other pulse shaping schemes presented in [4], where there is a reduction of PAPR about 4dB for $N = 8$ and $M = 8$ compared to rectangular pulse shaping.

REFERENCES

[1] C. An and H. Ryu, "Design and Performance Evaluation of Spectral Efficient Orthogonal Time Frequency Space System," 2019 IEEE 2nd 5G World Forum (5GWF), Dresden, Germany, 2019, pp. 249-252, doi: 10.1109/5GWF.2019.8911663.

[2] R. Hadani et al., "Orthogonal Time Frequency Space Modulation," 2017 IEEE Wireless Communications and Networking Conference (WCNC), San Francisco, CA, USA, 2017, pp. 1-6, doi: 10.1109/WCNC.2017.7925924.

[3] R. Hadani and A. Monk. (2018). "OTFS: A new generation of modulation addressing the challenges of 5G". [Online]. Available: https://arxiv.org/pdf/1802.02623.pdf

[4] G. D. Surabhi, R. M. Augustine and A. Chockalingam, "Peak-to-Average Power Ratio of OTFS Modulation," in IEEE Communications Letters, vol. 23, no. 6, pp. 999-1002, June 2019, doi: 10.1109/LCOMM.2019.2914042.

[5] R. M. Augustine and A. Chockalingam, "Interleaved Time-Frequency Multiple Access Using OTFS Modulation," 2019 IEEE 90th Vehicular Technology Conference (VTC2019-Fall), Honolulu, HI, USA, 2019, pp. 1-5, doi: 10.1109/VTCFall.2019.8891404.

[6] C. Naveen and V. Sudha, "Peak-to-Average Power Ratio reduction in OTFS modulation using companding technique," 2020 5th International Conference on Devices, Circuits and Systems (ICDCS), Coimbatore, India, 2020, pp. 140-143, doi: 10.1109/ICDCS48716.2020.243567.

[7] S. Gao and J. Zheng, "Peak-to-Average Power Ratio Reduction in Pilot-Embedded OTFS Modulation Through Iterative Clipping and Filtering," in IEEE Communications Letters, vol. 24, no. 9, pp. 2055-2059, Sept. 2020, doi: 10.1109/LCOMM.2020.2993036.

[8] P. Raviteja, Y. Hong, E. Viterbo and E. Biglieri, "Practical Pulse-Shaping Waveforms for Reduced-Cyclic-Prefix OTFS," in IEEE Transactions on Vehicular Technology, vol. 68, no. 1, pp. 957-961, Jan. 2019, doi: 10.1109/TVT.2018.2878891.

[9] P. Raviteja, K. T. Phan, Y. Hong and E. Viterbo, "Interference Cancellation and Iterative Detection for Orthogonal Time Frequency Space Modulation," in IEEE Transactions on Wireless Communications, vol. 17, no. 10, pp. 6501-6515, Oct. 2018, doi: 10.1109/TWC.2018.2860011.

[10] A. Farhang, A. RezazadehReyhani, L. E. Doyle and B. Farhang-Boroujeny, "Low Complexity Modem Structure for OFDM-Based Orthogonal Time Frequency Space Modulation," in IEEE Wireless Communications Letters, vol. 7, no. 3, pp. 344-347, June 2018, doi: 10.1109/LWC.2017.2776942.

[11] Tiwari S, Das SS (2019) Circularly pulse shaped orthogonal time frequency space modulation. Electron Lett. arXiv:1910.10457 ([cs.IT] 23 Oct 2019).

[12] N. C. Beaulieu and M. O. Damen, "Parametric construction of Nyquist-I pulses," in IEEE Transactions on Communications, vol. 52, no. 12, pp. 2134-2142, Dec. 2004, doi: 10.1109/TCOMM.2004.838739.

[13] Kamal, S., Azurdia-Meza, C.A. & Lee, K. Improved Nyquist-I Pulses to Enhance the Performance of OFDM-Based Systems. Wireless Pers Commun 95, 4095–4111 (2017). https://doi.org/10.1007/s11277-017-4044-3